Quantitative Characterization of Autoimmune Uveoretinitis in an Experimental Mouse Model

Jian Li,[1] Jialin Ren,[2] Yolanda Wong Ying Yip,[1] Xiaoyu Zhang,[1] Kai On Chu,[1] Tsz Kin Ng,[1] Sun On Chan,[2] Chi Pui Pang,[1] and Wai Kit Chu[1]

[1]Department of Ophthalmology & Visual Sciences, The Chinese University of Hong Kong, Hong Kong, People's Republic of China
[2]School of Biomedical Sciences, The Chinese University of Hong Kong, Hong Kong, People's Republic of China

Correspondence: Wai Kit Chu, Department of Ophthalmology & Visual Sciences, The Chinese University of Hong Kong, Hong Kong Eye Hospital, 147K Argyle Street, Kowloon, Hong Kong;
waikit@cuhk.edu.hk.

Submitted: June 14, 2017
Accepted: July 14, 2017

Citation: Li J, Ren J, Yip YWY, et al. Quantitative characterization of autoimmune uveoretinitis in an experimental mouse model. *Invest Ophthalmol Vis Sci*. 2017;58:4193–4200. DOI:10.1167/iovs.17-22436

Purpose. To accurately evaluate the autoimmune inflammation, we aim to develop three quantitative measurements to monitor the inflammatory changes in the retina: retinal-choroidal thickness, major retinal vessel diameter, and electroretinography amplitudes.

Methods. During a 21-day experimental period, eyes were examined by confocal scanning laser ophthalmoscopy, optical coherence tomography, fundus fluorescein angiography, and electroretinography in living mice, which were then subsequently killed for histologic assessments.

Results. On day 21 postimmunization, inflammation was observed both in vivo and in vitro. Fold change of retinal-choroidal thickness and major retinal vessel diameter in experimental autoimmune uveoretinitis mice were significantly greater than controls ($P < 0.001$). Both scotopic and photopic electroretinography amplitudes were significantly attenuated when compared with control mice ($P < 0.01$). Our results showed that these three quantifiable indicators provided an objective and accurate evaluation of autoimmune inflammation, which are in good correlations with the reported clinical and histopathologic scoring systems ($P < 0.05$).

Conclusions. These three indicators will be useful to detect the small but significant differences in the severity of experimental autoimmune uveoretinitis for future longitudinally therapeutic studies.

Keywords: uveitis-clinical/animal model, imaging, autoimmune disease

Uveitis is characterized by intraocular inflammation with extraocular manifestations in some individuals. It is a common and sight-threating disease that affects mainly young people aged 20 to 50 years.[1] Approximately 25% of irreversible blindness in developing countries is caused by uveitis.[2–4] Following the International Uveitis Study Group classification system,[5] uveitis is classified as anterior, intermediate, posterior, and panuveitis according to the anatomic location of the inflammatory process. Etiologically, uveitis can also be categorized as infectious and noninfectious. Infectious uveitis is generally more common in the developing world, accounting for 30% to 50% of all cases of uveitis.[2] If the infecting organisms are known, infectious uveitis can be managed specifically with anti-infective treatments. Noninfectious uveitis is characterized by considerable prevalence in the developed countries.[6] It is assumed to be an autoimmune or immune disorder. To control the autoimmune inflammation, the major therapeutic strategies are steroids and immune suppressants.

To mimic the human chronic autoimmune disorders, Caspi et al.[7] successfully induced experimental autoimmune uveoretinitis (EAU) in mice by injecting interphotoreceptor retinoid-binding protein, which serves as an autoantigen. After injection of the autoantigen into susceptible animals, activation of the retina-specific T cells that recognize the autoantigen was driven by the complete Freund's adjuvant. Consequently, the activated T cells broke through the vascular junctions of the blood–ocular barrier and infiltrated the ocular tissues. These T cells recognize the specific antigens in the eye and respond by secreting various cytokines and chemokines that eventually trigger the inflammatory cascade.[8–12] EAU is characterized largely by changes in the posterior chamber, including the presence of vitreal inflammatory cells, chorioretinal infiltrates (granulomas), retinal vessel inflammation (retinal vasculitis), and oedema (optic nerve, exudative retinal detachment).

Semiquantifiable scoring systems based on morphologic observations from both fundoscopy and histologic verification in EAU studies have led to many important findings.[13] Criteria for grading EAU include inflammatory cell infiltrations, vasculitis, chorioretinal lesions, and retinal folds.[14,15] The graders' experience, however, affects the accuracy of scores. Variations arise from interpersonal imprecision or subjective bias. Recently, in vivo methods, such as bioluminescence imaging, were used to achieve higher resolution analyses in several uveitis animal models. However, EAU was still difficult to quantify.[16,17] Optical coherence tomography (OCT) is a noninvasive in vivo imaging modality that provides structural information with resolution at micrometer level and can be performed repeatedly on living animals. Retinal OCT has been described for use in EAU previously to show the retinal changes.[18–21] Nevertheless, quantifiable systems for the evaluation of OCT images are required. Confocal scanning laser ophthalmoscopy (cSLO) based fundus fluorescein angiography (FFA), another in vivo imaging method, is now available and is capable of revealing inflammatory changes of retinal blood

Copyright 2017 The Authors

This work is licensed under a Creative Commons Attribution-NonCommercial-NoDerivatives 4.0 International License.

Downloaded from iovs.arvojournals.org on 12/04/2020

vessels, including the dilated vessel size and vessel leakage. Furthermore, electroretinography (ERG) indicates the visual function affected in both autoimmune uveitis patient and EAU animals.[18,22,23] It could be used as an objective and quantifiable testing method. The present study aims to establish a system with multiple quantifiable indicators to characterize inflammatory changes in a mouse model of EAU by using various in vivo techniques and to be more sensitive and reliable than previously reported methods to detect small phenotypic changes associated with uveitis in living animals.

Materials and Methods

Animals and Induction of Experimental Autoimmune Uveitis

Female C57BL/6J mice, aged 6 to 8 weeks, were obtained from the Laboratory Animal Service Center, Faculty of Medicine, The Chinese University of Hong Kong. All animals were housed in a specific pathogen-free facility at 20°C with 12/12 hour light–dark cycles and allowed to freely access food and water. All experiments were conducted according to the ARVO Statement for the Use of Animals in Ophthalmic and Vision Research. Ethics approval for this study was obtained from the Animal Experimentation Ethics Committee of The Chinese University of Hong Kong.

Two independent cohorts of mice (18 and 8 mice, respectively) were injected subcutaneously with human interphotoreceptor retinoid-binding protein peptide 1-20 (GPTHLFQPSLVLDMAKVLLD; Anapec, Inc., San Jose, CA, USA) emulsified 1:1 volume/volume (v/v) in complete Freund's adjuvant containing 4.5 mg/mL *Mycobacterium tuberculosis* H37RA (Difco, Detroit, MI, USA). A total of 200-μL emulsion was injected subcutaneously along the base of the tail (100 μL) and both thighs (50 μL each). In all immunizations, pertussis toxin (0.1 μg in 100 μL; Catalog Number P7208; Sigma-Aldrich Corp., St. Louis, MO, USA) was injected intraperitoneally on the day of immunization, as described previously.[13,14] Two corresponding groups of control animals with 18 and 8 mice, respectively, were injected both subcutaneously into tail and thighs and intraperitoneally with an equal volume of sterile PBS. The first cohort of mice (18 EAU mice and 18 controls) was subjected to all the measurements employed in this study. The second cohort of mice (8 EAU mice and 8 controls) was subjected to repeat the measurements of retinal-choroidal thickness, major retinal vessel diameter, and ERG in the longitudinal investigations.

In Vivo Imaging by cSLO

To prepare for the cSLO imaging, the mice were anesthetized by intraperitoneal injection of ketamine (75 mg/kg) and xylazine (10 mg/kg). Pupils were dilated with topical mydriatic agents (tropicamide and phenylephrine, 0.5% each) to approximately 2 mm in diameter. The imaging procedure followed that described in our earlier reports.[24,25] Prior to imaging, the mice were anesthetized and immediately placed on a custom-made platform. The head was fixed in position for imaging. During imaging, sterile artificial tears (Alcon, Inc., Puurs, Belgium) were applied to the cornea every 2 minutes to maintain media clarity. In cSLO (Heidelberg Retina Angiograph 2 [HRA2]; Heidelberg Engineering GmbH, Dossenheim, Germany), the cSLO infrared reflectance was recorded using a light source with 820-nm wavelength to provide planar visualization of the retina. The scan rate was 16 frames per second. Eye tracking (a retinal recognition technology enabling the exact same retinal location to be "locked on" and scanned) was activated during image acquisition. A 55° widefield noncontact lens (Heidelberg Engineering GmbH) was added to the camera to capture high-quality images in a wider view of the fundus. A total of 15 images at the same retinal location at the same focal depth were captured and averaged automatically by the built-in software to increase the signal-to-noise ratio with simultaneous display on computer screen. Each image frame represents approximately 40% of the total retinal area.[26,27] We took 9 images on sequential regions to cover both central and periphery retina. Clinical scoring was performed in a blinded manner by selecting the most severe example of inflammation present and marked on a scale of 0 to 4, as described previously.[13]

In Vivo Imaging by Spectral-Domain OCT

The OCT system used a superluminescent diode light source with a center wavelength of 870 μm. OCT parameters were modified to adapt OCT imaging in mice according to the manufacturer instruction (Heidelberg Engineering GmbH). Thus, infrared retinal fundus photographs and OCT images could be simultaneously captured on the exact retinal locus, which ensures the high quality of OCT imaging in the retina. In each retina, a square region centered on the optic nerve head were covered by 19 OCT cross-sections.[28] Nine images for each B-scan at the same retinal location were captured and averaged. For quantification of retinal-choroidal thickness, we used the software package from Heidelberg Engineering. By correlating the OCT image with histologic section, we defined the distance from the vitreo-retinal interface to the choroid-sclera interface as the retinal-choroidal thickness (RCT). The RCT data were shown in a form of Early Treatment of Diabetic Retinopathy Study (ETDRS) grid, which centered on optic disc. Each number represents the averaged thickness data in the specific region. The central data was excluded due to the absence of retina and choroid at the optic nerve head. The fold change of RCT compared with the baseline RCT was calculated and is presented as mean ± standard error of mean.

Fundus Fluorescein Angiography

For FFA, 100 μl of 10% fluorescein (Fluorescite, Alcon Laboratories, Fort Worth, TX, USA) was injected intraperitoneally, and cSLO examination was performed within 5 seconds after the fluorescein injection. FFA images were analyzed using a built-in software to measure the diameter of major retinal vessels at 5000 units away from the center of the optic disc. Major retinal vessels are defined by those vessels originated from the optic nerve head and reaching the boundaries of the fundus photos. Total major retinal vessel diameters of each mouse were then averaged by the number of major retinal vessels for statistical analyses. Fluorescein signals of microvasculature and branch of major retinal vessels were excluded for the measurement.

Electroretinography

Mice were dark adapted at least 12 hours prior to ERG recordings. Mice were anesthetized and pupils dilated using the same protocol as in the in vivo imaging. A gold ring electrode was placed on the cornea with reference in the mouth and ground electrode inserted subcutaneously into the hind leg. Body temperature was maintained at 37°C with a heated pad during recording and all the procedures were performed in a dark room with a dim red light. Visual function was tested by recording scotopic and photopic ERG with a Diagnosys Espion system and the ColorDome light emitting

Investigative Ophthalmology & Visual Science

Downloaded from iovs.arvojournals.org on 12/04/2020

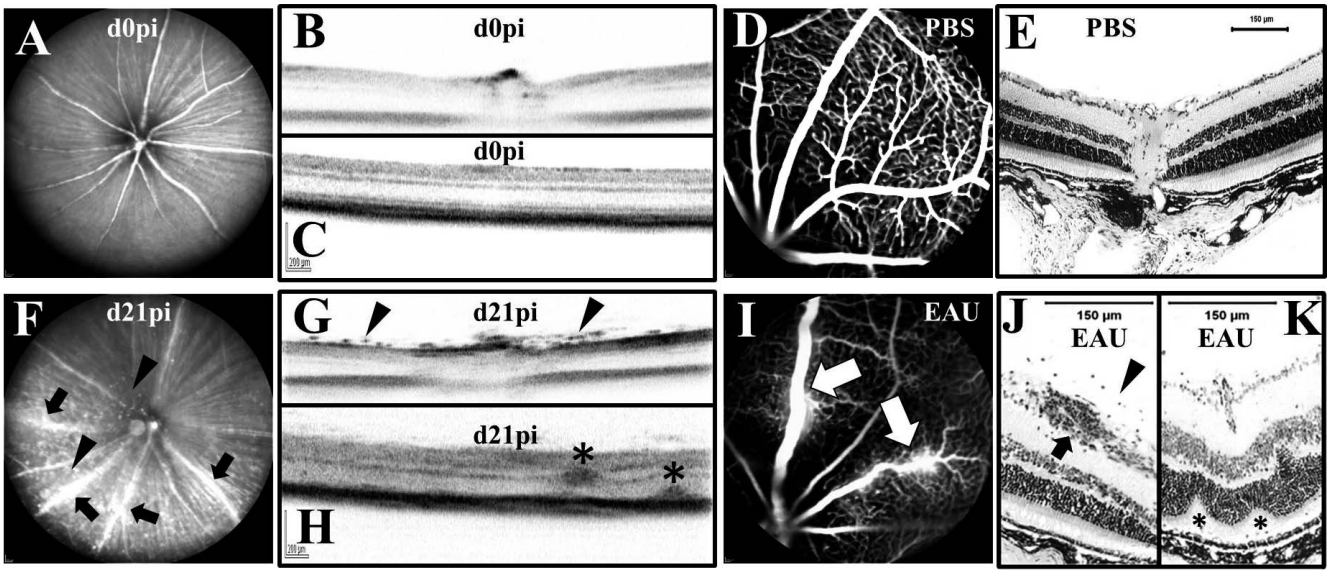

FIGURE 1. In vivo imaging and in vitro histologic analyses for the detection of vital signs of retinal changes associated with EAU in C57BL/6 mice. Animals before EAU induction (day 0) had normal cSLO (**A**) and OCT (**B**, **C**) appearances. (**F**–**H**) Matched images from mice at day 21 postimmunization of EAU demonstrated detectable changes. Vitreous of EAU mice were densely infiltrated with inflammatory cells (*arrow heads*). cSLO image (**F**) clearly identified severe vasculitis (*arrows*). OCT cross-sections (**G**, **H**) showed retinal structural disruptions (*asterisks*) and retinal edema. When compared with the control eye (**D**), vessel leakages (*white arrows*) in the EAU animal were presented in FFA images (**I**). Matched histology demonstrated inflammatory infiltrating cells (*arrow heads*), vasculitis (*arrows*), retinal folds, and detachment (*asterisks*) in EAU (**J**, **K**), but not control mice (**E**).

diode (LED) full-field stimulator (Diagnosys LLC, Lowell, MA, USA). The light intensity was calibrated by the manufacturer and was computer controlled. In the scotopic condition, ERGs were recorded under single white-flash stimulus with intensities ranging 0.001, 0.01, 0.1, 1, and 10 cd.s/m^2. Afterward, photopic ERG was recorded under stimulus intensities of 0.5, 1, 5, 10, and 30 cd.s/m^2 with a background light of 5 cd.s/m^2. For each stimulus, at least five responses were averaged with an interstimulus interval of 2 seconds. The amplitude of b-wave was measured from the trough of the a-wave to the peak of the b-wave.

Histology

On postimmunization day 21, under deep anesthesia, the mice were perfused intracardially with 0.01 M sterile PBS followed by 4% paraformaldehyde. Both eyes were removed and further immersed in 4% paraformaldehyde for 24 hours at 4°C. Connective tissues were maintained on each eye to facilitate orientation. The eyes were embedded in paraffin and sectioned in 5-µm thickness along the vertical meridian and the optic nerve head. After deparaffinization and rehydration, the sections were stained with hematoxylin and eosin. The anterior and posterior segments of the eyeball were examined under a light microscope (DMRB, Leica Microsystems, Wetzlar, Germany) connected to a Spot digital camera (Diagnostic Instrument, Inc., Sterling Heights, MI, USA). Based on the number, type, and size of lesion, histopathologic disease scores were assigned on a scale of 0 to 4 using published criteria by a colleague who is blinded to the sample numbers and grouping.[13]

Statistical Analysis

All data are expressed as mean ± standard error of mean (SEM). SPSS version 19.0 (IBM Corp., Armonk, NY, USA) and GraphPad Prism 5.0 (GraphPad Software, Inc., La Jolla, CA, USA) software were used for the statistical analysis. Nonparametric Mann-Whitney *U* test was used to compare the medians of two groups and at different time points. To compare the differences before and after EAU induction in individuals, Wilcoxon signed-rank test was performed. Spearman's correlation analysis was used to evaluate the relationship between two parameters. All statistical tests were two-tailed and were performed using a significance level of $P = 0.05$.

RESULTS

In Vivo Imaging and Histologic Analysis for the Detection of Retinal Changes Associated With EAU in C56BL/6 Mice

Spectral-domain OCT (SD-OCT) and cSLO images were obtained on day 0 (baseline) and day 21 (endpoint) for 18 animals, which were equally and randomly divided into EAU group and control group (mock induced with PBS). FFA was performed on day 21 for a clear visualization of retinal vasculature prior to killing the animals for histopathologic verification.

In control animals, cSLO revealed clearly the optic nerve, retinal vessels, and nerve fibers in the retina (Fig. 1A). OCT cross-sectional B-scans resolved the characterized retinal layers, including the retinal nerve fibers/ganglion cell layer, inner plexiform layer, inner nuclear layer, outer plexiform layer, outer nuclear layer, inner/outer segments (IS/OS) of rods and cones, retinal pigmented epithelium, and choroid, corresponding to the respective layers of the histologic section of the retina (Supplementary Fig. S1).

A comparison of images from day 0 (Figs. 1A–C) and day 21 (Figs. 1F–H) revealed inflammatory morphologic changes of EAU, including infiltrating cells in the vitreous, vasculitis, retinal structural disruption, and retinal edema.

In EAU mice, FFA on day 21 enhanced the vasculature display and identified vessel leakage (Fig. 1I) along with the

Investigative Ophthalmology & Visual Science

Downloaded from iovs.arvojournals.org on 12/04/2020

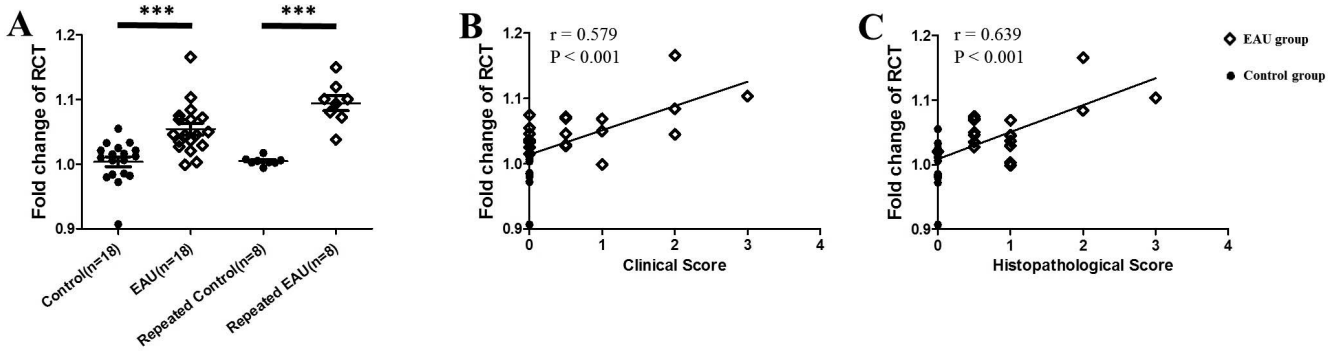

FIGURE 2. Quantitative measurement of RCT by SD-OCT detects inflammatory edema. (**A**) Retinal-choroidal thickness (RCT) at day 21 postinduction of EAU was divided by that at baseline (day 0) to assess the fold change of RCT caused by EAU. Each point shows the data of individual subject. Statistics are evaluated by Mann-Whitney *U* test (***$P < 0.001$). SEMs are shown. (**B**, **C**) Spearman rank correlation coefficients are displayed for comparisons between fold change of RCT against clinical and histopathologic scores, respectively.

appearance of optic disc swelling (papilledema; Supplementary Fig. S2) caused by EAU. We have compared the same eye using in vivo imaging and histologic sections in EAU and control mice. In correlation with in vivo findings, histopathology detected vitritis, vasculitis, choroiditis, retinal detachment, granuloma, retinal folds, and edema only in the EAU mice (Figs. 1J–K). Furthermore, signs of inflammation were not observed in SD-OCT images or by histology in control mice. Inflammation was scored both clinically (0.81 ± 0.21) and histopathologically (0.97 ± 0.17) for EAU mice, whereas the clinical and histopathologic scores were both zero in control mice ($P < 0.001$ when compared with the respective clinical and histopathologic scores in EAU mice; Supplementary Fig. S3).

Quantitative Measurement of RCT by SD-OCT Detects Inflammatory Edema

Retinal-choroidal thickness was determined by SD-OCT in EAU mice on day 0 and day 21 after EAU induction. An ETDRS grid centered on optic disc displayed the RCT data (Supplementary Fig. S4). For comparison, numbers in eight areas for day 0 and day 21 after EAU induction were averaged, and we found significantly higher fold changes of RCT in EAU mice during the 21-day period (1.054 ± 0.010) than control mice (1.004 ± 0.008, $P < 0.001$). Consistent differences were obtained in a repeated experiment, 1.094 ± 0.012 in EAU against 1.005 ± 0.002 in controls, $P < 0.001$ (Fig. 2A).

The increase of RCT was also significantly correlated with the severity of EAU shown by clinical scores (Spearman $r = 0.579$, $P < 0.001$, 95% confidence interval [CI]: 0.328 to 0.795) and histopathologic scores (Spearman $r = 0.639$, $P < 0.001$, 95% CI: 0.355 to 0.841; Figs. 2B–C). Thus, we propose the RCT could be employed as an indicator for quantitative characterization in EAU mice.

Quantitative Assessment of the Major Retinal Vessel Diameter Identifies Vasodilation in Association With Inflammation

Fluorescein was intraperitoneally injected into the animals to reveal the retinal vasculature for precise measurements, especially the superficial layer vessels (Fig. 3A). On average, EAU animals showed significantly greater vessel diameters (296.15 ± 6.15 units) when compared with controls (244.62 ± 8.17 units, $P < 0.001$), indicating vasodilation caused by the inflammation. To verify this novel indicator, we performed another repeated experiment. Consistent results were obtained. The major retinal vessel size in EAU mice (310.84 ± 10.47 units) was also significantly greater than controls (224.35 ± 5.50 units, $P < 0.001$; Fig. 3B).

Similar to the RCT, major vessel diameters also correlated with the clinical scores (Spearman $r = 0.580$, $P < 0.001$, 95% CI: 0.319 to 0.775) and the histologic scores (Spearman $r = 0.574$, $P < 0.001$, 95% CI: 0.298 to 0.792; Figs. 3C–D). Therefore, the major retinal vessel diameter could be employed as a quantifiable indicator for the evaluation of the EAU severity. Moreover, the major vessel diameter also showed significant correlation with RCT (Spearman $r = 0.552$, $P < 0.001$, 95% CI: 0.254 to 0.792), which means both indicators could be used to reliably quantify the severity of EAU (Supplementary Fig. S5).

ERG Amplitudes Indicate Visual Function Loss in EAU Mice

To examine whether the inflammatory changes would lead to visual function disruption, an ERG recording system was used to compare the functional changes in EAU and control mice during the experimental periods. In an intragroup comparison of the ERGs on day 0 and day 21, we found detectable reduction in both photopic (light-adapted) and scotopic (dark-adapted) b-wave, but not a-wave, amplitudes under all tested intensities of light stimulus ($P < 0.01$; Figs. 4A, 4D), implying retina related visual signaling pathway impairment. In a further analysis of intergroup comparison (EAU mice vs control mice), we found the relative photopic and scotopic ERG amplitudes, calculated as the ratio of amplitudes at day 21 and day 0 under the strongest light stimulus, in the EAU group (81.48% ± 3.86% and 77.20% ± 5.15%, respectively) were also significantly attenuated when compared with controls (106.38% ± 4.50% and 97.87% ± 3.69%, respectively, $P < 0.01$; Figs. 4G–H).

We found no significant correlation between photopic ERGs and clinical score (Spearman $r = -0.225$, $P = 0.187$, 95% CI: –0.551 to 0.126; Fig. 4B). Associations between photopic ERGs with histologic score, scotopic ERGs with clinical score, and scotopic ERGs with histologic score (Spearman r ranged between –0.391 to –0.601) showed statistical significance ($P < 0.05$), which confirmed that animals with more severe inflammation have lower visual function (Figs. 4C, 4E–F). Herein, besides the morphologic monitoring, ERG confirmed the functional loss of retinal cells induced by EAU and provides quantifiable parameters for the quantitative evaluation system.

Downloaded from iovs.arvojournals.org on 12/04/2020

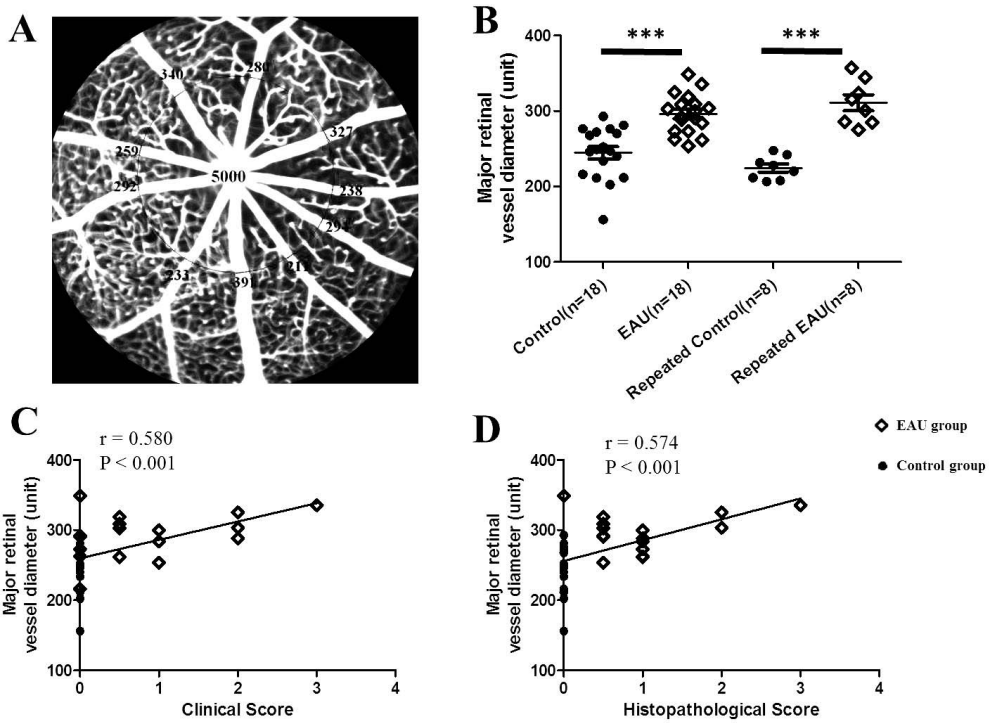

FIGURE 3. Quantitative assessment of the major retinal vessel diameter identifies vasodilation in association with inflammation. (**A**) Diameters at a specific position 5000 units away from the center of optic disc were manually measured for each major vessel. Fluorescein signals of microvasculature and branch of major retinal vessels were excluded for the measurement. (**B**) Major retinal vessel diameter assessments for each vessel were averaged for presentation of an individual mouse. Each point shows the data of individual subject. Statistics are evaluated by Mann-Whitney *U* test (***$P < 0.001$). SEMs are shown. (**C**, **D**) Spearman rank correlation coefficients are displayed for comparisons between major retinal vessel diameter against clinical and histopathologic scores, respectively.

Longitudinal Assessments of RCT and ERG Responses in Living Mice

EAU animals were monitored by OCT and ERG on baseline (day 0), day 14, and day 21 postimmunization. Fold change of RCT in EAU mice was significantly increased on day 21 (1.075 ± 0.015, $P < 0.001$), but not on day 14 (1.019 ± 0.003, $P > 0.05$), compared to that in control animals (1.004 ± 0.004 and 1.002 ± 0.008, respectively; Fig. 5A). ERG amplitudes, both photopic and scotopic, decreased progressively during the 21-day development of EAU (Figs. 5B–C). Thus, the in vivo measurements of RCT and ERG responses can longitudinally assess the inflammatory status in mouse eyes.

DISCUSSION

In the present study, to quantitatively characterize the autoimmune ocular inflammation in a mouse model of EAU, we employed three quantifiable indicators—RCT, major retinal vessel diameter, and ERG amplitudes—generated by OCT, cSLO/FFA, and ERG, respectively. The results showed significant correlations with histologic and clinical scores. We conclude that these three indicators, in addition to the semiquantifiable grading systems, can reliably and quantitatively characterize the small but significant differences in the severity of retinal inflammation in EAU mice, which could be useful for longitudinal therapeutic studies.

The retina is a major target of autoimmune responses. It is commonly monitored by color fundus photography. cSLO is a laser-sourced technique providing higher transverse resolution of white–black fundus photos. We combined it with SD-OCT in a HRA2 imaging system to achieve simultaneous capture of fundus and OCT images on the exact retinal focus. Therefore, OCT sections can be precisely located to the lesion site under direct visualization of cSLO views. In the present study, morphologic changes on the retina of EAU mice could be observed on cSLO images, including the infiltrating cells in the vitreous, vasculitis, retinal lesion, and detachment. With the injection of fluorescein dye into the animal, FFA images can also be obtained by the cSLO system, which clearly showed the vessel leakage and papilledema. However, three-dimensional information, such as retinal edema and structural changes within the retina, is lost in two-dimensional fundus photos. To complement with the thicknesses in the retina and choroid, OCT could be used along with the fundus photos. OCT is noninvasive and can be repeatedly used in individual animals noninvasively. Therefore, we combined the cSLO and OCT-HRA2 imaging system to monitor the inflammatory changes in our experiments.

We performed the semiquantifiable scorings by using reported grading systems in EAU mice and found low EAU scores, mainly 1 out of 4. For example, some of the animals in EAU group were scored with 0 because of the absence of signs listed in the scoring systems. In the current study, our EAU mice showed a clinical score of 0.81 ± 0.21 on day 21 postimmunization. The C57BL/6 mouse strain is well known for its moderate susceptibility to EAU induction, which is more closely related to human uveitis in terms of its chronic and longer disease duration.[7,13] In several cases, the EAU mice showed small but distinguishable clinical and histologic differences, which were not sufficiently significant to be categorized into higher grades in the scoring systems. Therefore, sensitivity issues may arise in drug screening studies, as the scales of grading systems are not precise enough to show the small therapeutic effects, which have been

Investigative Ophthalmology & Visual Science

Downloaded from iovs.arvojournals.org on 12/04/2020

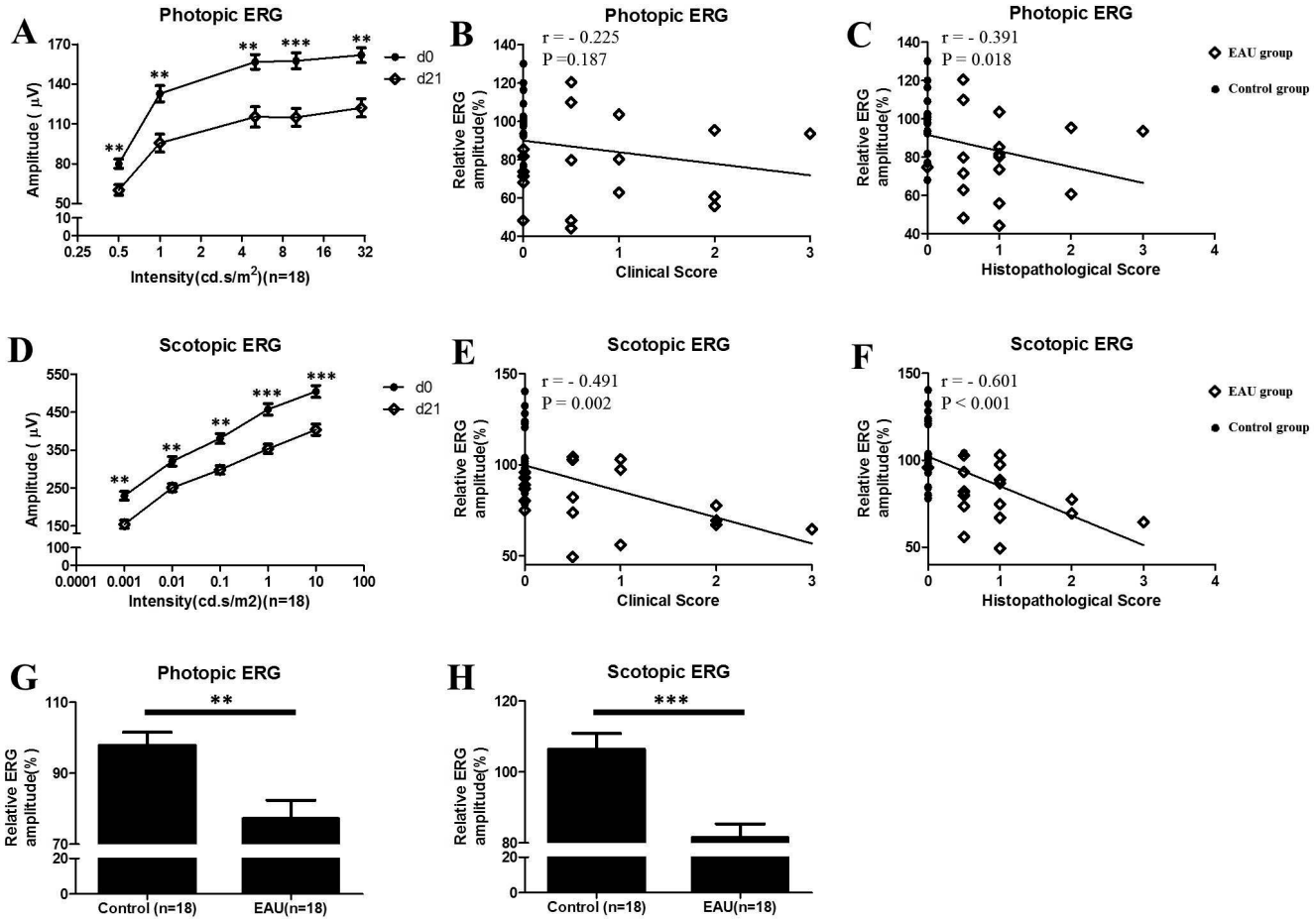

FIGURE 4. ERG amplitudes indicate visual function loss in EAU mice. (**A**, **D**) Photopic and scotopic ERG amplitudes of EAU mice at day 0 and day 21 were compared. (**G**, **H**) ERG amplitudes were compared between controls and EAU animals. Relative ERG amplitudes were calculated as the ratios of amplitudes at day 21 and day 0 under the strongest light stimulus. Statistics are evaluated by Mann-Whitney *U* test for independent comparisons (**G**, **H**) and Wilcoxon signed-rank test for paired comparisons (**A**, **D**; $^{**}P < 0.01$, $^{***}P < 0.001$). SEMs are shown. (**B**, **C**, **E**, **F**) Spearman rank correlation coefficients are shown for comparisons between relative ERG amplitudes against clinical and histopathologic scores, respectively.

demonstrated in previous publications.[29] Moreover, these scoring systems highly depend on graders' experience. Recently, a quantitative bioluminescence assay has been introduced to evaluate intraocular inflammation in two acute models primed mycobacterial uveitis and endotoxin-induced uveitis.[16] No significant changes were detected in EAU mice.

Based on clinical observations, retina and choroid thickening is an important feature in uveitis patients as a result of inflammatory edema.[30,31] We noticed retinal thicknesses, excluding the choroidal thickness, on one optic disc diameter away from the two edges of the optic disc, which have lower representation of the average retinal thickness, have been reported in evaluating EAU in previous publications.[18,20] Because both the retina and choroid are involved in the inflammatory process of the pathogenesis of EAU, we measured the retinal-choroidal thickness as an indicator to reflect the severity of EAU. To enhance the accuracy, we used 19 OCT sections to cover the retina centered on the optic disc and measure RCT on each scan. Subsequently, the RCT can be presented by the ETDRS grid. Each of the nine numbers represents the averaged thickness data in the respective region. The data in the central circle of the ETDRS grid was excluded because of the loss of retina/choroid at the optic nerve head. The mean fold change of RCT in EAU mice was significantly higher than that in normal control eyes. The RCT measurement quantified the initially subjective observation of inflammatory retinal edema. To verify the reproducibility of this novel indicator, a repeated study was conducted and consistent results obtained. This indicator is thus capable of distinguishing EAU animals from normal controls. To further test its agreement with previous scoring system results, the fold change of RCT was significantly correlated with both clinical score and histologic score, which means the RCT has the ability to determine the severity of EAU as well as the grading systems.

Besides the inflammatory retinal edema, vasodilation caused by vasculitis is another common symptom in uveitis patients.[32] Semiquantifiable scoring systems are available to evaluate the vessel size as a criterion for severity scores. Herein, we quantified the retinal vessel diameter as the second indicator. For high-quality retinal vasculature images, FFA was acquired by cSLO with fluorescein injection. However, cSLO is limited by the two-dimensional imaging technology, which means that only one retinal layer can be captured on a single focal plane. Thus the major vessels in superficial layer were focused for imaging. The retinal vessel diameter at the position of 5000 units away from center of optic disc was determined. To minimize the variation of individual vasculature and background noise caused by deeper layer microvasculature, branches of major vessels and fluorescein signals of tiny vessels were excluded. The averages of individual major vessel diameters were calculated for each animal. Our results showed

Investigative Ophthalmology & Visual Science

Downloaded from iovs.arvojournals.org on 12/04/2020

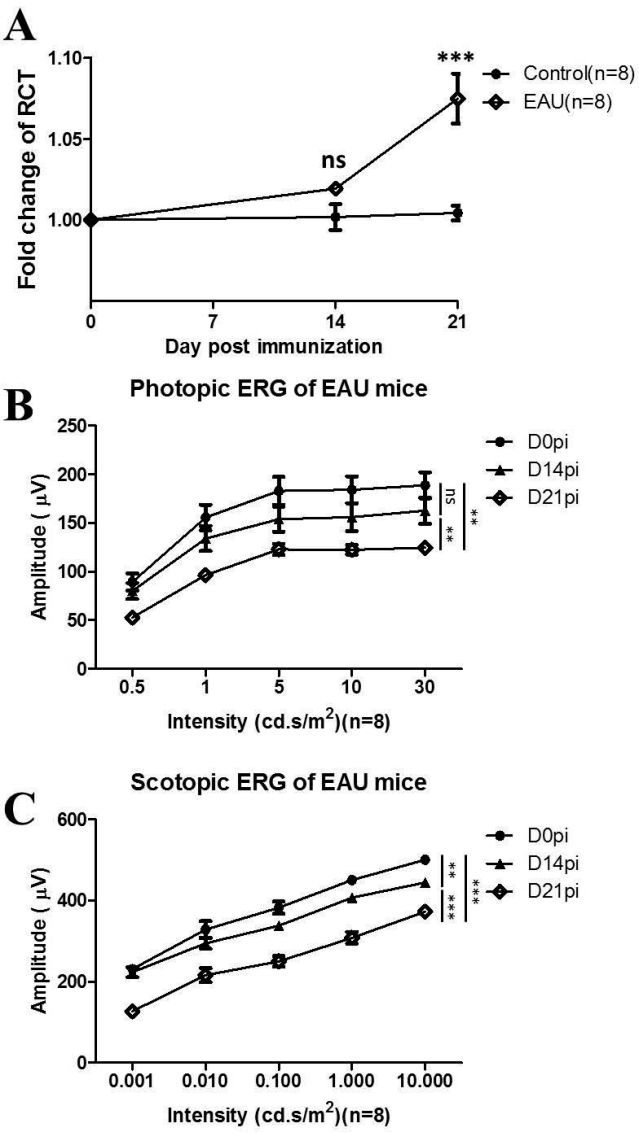

FIGURE 5. Longitudinal assessments of RCT and ERG responses in living mice. (**A**) Fold change of RCT observed by OCT on day 0, day 14, and day 21. (**B**, **C**) Photopic and scotopic ERG responses on day 0, day 14, and day 21. Data are presented as mean ± SEM. Statistics are evaluated by Mann-Whitney *U* test for independent comparisons (**A**) and Wilcoxon signed-rank test for paired comparisons (**B**, **C**; $^{**}P < 0.01$, $^{***}P < 0.001$, ns = no significance).

vasodilation by enlarged vessel size in EAU animals, which is consistent with reported clinical observation in autoimmune uveitis patients.[33,34] Interestingly, the correlations between major retinal vessel diameters and grading scores were not as high as that of RCT. As fluorescein injection might cause animal death, FFA was only performed on day 21 postimmunization (endpoint). When compared with the fold changes of RCT standardized by baseline, actual major vessel diameter values, instead of fold changes, were used for analyses to generate larger variation between individuals, leading to lower correlation with grading scores when compared with RCT. Nevertheless, the major vessel diameter was still significantly correlated with grading scores ($P \leq 0.001$) and RCT ($P < 0.001$), which confirmed its accuracy in quantitative evaluation of the EAU.

Declining vision commonly occurs in posterior uveitis patients. In this study, we employed ERG to assess the visual function in EAU mice. Reduction of dark- and light-adapted ERGs during EAU development was reported previously.[18,35] To improve sensitivity and accuracy, we recorded the ERG amplitudes under five different light intensities in both scotopic and photopic recordings. Scotopic response reflects the rod cell-related activities, whereas the photopic recording represents the visual function associated with cone cells. Our observation of the sharp ERG loss during EAU development is consistent with the visual impairment in previous publications.[18] By correlating with the grading scores, scotopic ERGs significantly reduced in high-score individuals. However, correlations between photopic responses and grading scores were not highly significant although a trend of negative correlation was observed. Notably, even though most of the C57BL/6 EAU mice had low grading scores indicating mild morphologic changes, the ERG amplitudes attenuated dramatically by the EAU induction. Therefore, ERG could be a more sensitive method in evaluating the severity of EAU.

In our evaluation of the quantifiable indicators and established severity scorings, we found the absolute values of Spearman rank correlation coefficients ranged from 0.391 to 0.639. These moderate correlations could be explained by the different perspectives of the two evaluation systems. Each of our quantifiable indicators specifically assessed one aspect of the disease. However, the previous scoring systems comprehensively evaluate the animals based on different aspects of the disease including lesions, infiltrations, vasculitis, retinal detachment, and atrophy. Similar to uveitis patients, inflammatory signs vary in individual animals. However, even though the two different evaluation systems were not highly correlated with each other, the statistic significances still showed consistent effects between them. Thus, the two systems should work together complimentarily for quantification of ocular inflammation.

The EAU mouse model as a platform for investigation of autoimmune ocular inflammation has been reported since 1988.[7] The well-established semiquantifiable scoring systems contributed to numerous important discoveries in ocular immunology, leading to many therapies for ocular autoimmune inflammation. Our current study, correlated with the grading systems, is the first to establish a novel quantitative and real-time evaluation system for a mouse EAU model. The three quantifiable indicators, RCT, major retinal vessel diameter, and ERG amplitudes, provide a more objective and accurate evaluation of autoimmune inflammation for longitudinally therapeutic studies using this model.

Acknowledgments

The authors thank Pancy Tam for excellent technical support.

Supported by the Health and Medical Research Fund (Project 12130811 [CPP]), a Hong Kong Special Administrative Region (HKSAR) Research Grant Council General Research Fund (Project 14113815 [SOC]), and the Hospital Authority of Hong Kong.

Disclosure: **J. Li**, None; **J. Ren**, None; **Y.W.Y. Yip**, None; **X. Zhang**, None; **K.O. Chu**, None; **T.K. Ng**, None; **S.O. Chan**, None; **C.P. Pang**, None; **W.K. Chu**, None

References

1. Rothova A, Buitenhuis HJ, Meenken C, et al. Uveitis and systemic disease. *Br J Ophthalmol*. 1992;76:137–141.
2. Tsirouki T, Dastiridou A, Symeonidis C, et al. A focus on the epidemiology of uveitis. [published online ahead of print July 28, 2016]. *Ocul Immunol Inflamm*. doi:10.1080/09273948.2016.1196713.
3. Nussenblatt RB. The natural history of uveitis. *Int Ophthalmol*. 1990;14:303–308.

Investigative Ophthalmology & Visual Science

Downloaded from iovs.arvojournals.org on 12/04/2020

4. Rothova A, Suttorp-van Schulten MS, Frits Treffers W, Kijlstra A. Causes and frequency of blindness in patients with intraocular inflammatory disease. *Br J Ophthalmol*. 1996; 80:332–336.
5. Trusko B, Thorne J, Jabs D, et al.; for the Standardization of Uveitis Nomenclature (SUN) Project. Development of a clinical evidence base utilizing informatics tools and techniques. *Methods Inf Med*. 2013;52:259–265.
6. Rathinam SR, Namperumalsamy P. Global variation and pattern changes in epidemiology of uveitis. *Indian J Ophthalmol*. 2007;55:173–183.
7. Caspi RR, Roberge FG, Chan CC, et al. A new model of autoimmune disease. Experimental autoimmune uveoretinitis induced in mice with two different retinal antigens. *J Immunol*. 1988;140:1490–1495.
8. Caspi RR. A look at autoimmunity and inflammation in the eye. *J Clin Invest*. 2010;120:3073–3083.
9. Thurau SR, Mempel TR, Flugel A, et al. The fate of autoreactive, GFP+ T cells in rat models of uveitis analyzed by intravital fluorescence microscopy and FACS. *Int Immunol*. 2004;16:1573–1582.
10. Prendergast RA, Iliff CE, Coskuncan NM, et al. T cell traffic and the inflammatory response in experimental autoimmune uveoretinitis. *Invest Ophthalmol Vis Sci*. 1998;39:754–762.
11. Caspi RR, Roberge FG, McAllister CG, et al. T cell lines mediating experimental autoimmune uveoretinitis (EAU) in the rat. *J Immunol*. 1986;136:928–933.
12. Caspi RR, Chan CC, Fujino Y, et al. Recruitment of antigen-nonspecific cells plays a pivotal role in the pathogenesis of a T cell-mediated organ-specific autoimmune disease, experimental autoimmune uveoretinitis. *J Neuroimmunol*. 1993;47: 177–188.
13. Caspi RR. Experimental autoimmune uveoretinitis in the rat and mouse. *Curr Protoc Immunol*. 2003; chapter 15:unit 15.6.
14. Agarwal RK, Silver PB, Caspi RR. Rodent models of experimental autoimmune uveitis. *Methods Mol Biol*. 2012; 900:443–469.
15. Whitcup SM, DeBarge LR, Caspi RR, Harning R, Nussenblatt RB, Chan CC. Monoclonal antibodies against ICAM-1 (CD54) and LFA-1 (CD11a/CD18) inhibit experimental autoimmune uveitis. *Clin Immunol Immunopathol*. 1993;67:143–150.
16. Gutowski MB, Wilson L, Van Gelder RN, Pepple KL. In vivo bioluminescence imaging for longitudinal monitoring of inflammation in animal models of uveitis. *Invest Ophthalmol Vis Sci*. 2017;58:1521–1528.
17. Pepple KL, Choi WJ, Wilson L, Van Gelder RN, Wang RK. Quantitative assessment of anterior segment inflammation in a rat model of uveitis using spectral-domain optical coherence tomography. *Invest Ophthalmol Vis Sci*. 2016;57:3567–3575.
18. Chen J, Qian H, Horai R, Chan CC, Caspi RR. Use of optical coherence tomography and electroretinography to evaluate retinal pathology in a mouse model of autoimmune uveitis. *PLoS One*. 2013;8:e63904.
19. Harimoto K, Ito M, Karasawa Y, Sakurai Y, Takeuchi M. Evaluation of mouse experimental autoimmune uveoretinitis by spectral domain optical coherence tomography. *Br J Ophthalmol*. 2014;98:808–812.
20. Gadjanski I, Williams SK, Hein K, Sattler MB, Bahr M, Diem R. Correlation of optical coherence tomography with clinical and histopathological findings in experimental autoimmune uveoretinitis. *Exp Eye Res*. 2011;93:82–90.
21. Chu CJ, Herrmann P, Carvalho LS, et al. Assessment and in vivo scoring of murine experimental autoimmune uveoretinitis using optical coherence tomography. *PLoS One*. 2013;8: e63002.
22. Tzekov R, Madow B. Visual electrodiagnostic testing in birdshot chorioretinopathy. *J Ophthalmol*. 2015;2015: 680215.
23. Sobrin L, Lam BL, Liu M, Feuer WJ, Davis JL. Electroretinographic monitoring in birdshot chorioretinopathy. *Am J Ophthalmol*. 2005;140:52–64.
24. Yang Y, Ng TK, Ye C, et al. Assessing sodium iodate-induced outer retinal changes in rats using confocal scanning laser ophthalmoscopy and optical coherence tomography. *Invest Ophthalmol Vis Sci*. 2014;55:1696–1705.
25. Yang Y, Qin YJ, Yip YW, et al. Green tea catechins are potent anti-oxidants that ameliorate sodium iodate-induced retinal degeneration in rats. *Sci Rep*. 2016;6:29546.
26. Liu S, Li ZW, Weinreb RN, et al. Tracking retinal microgliosis in models of retinal ganglion cell damage. *Invest Ophthalmol Vis Sci*. 2012;53:6254–6262.
27. Li ZW, Liu S, Weinreb RN, et al. Tracking dendritic shrinkage of retinal ganglion cells after acute elevation of intraocular pressure. *Invest Ophthalmol Vis Sci*. 2011;52:7205–7212.
28. Guo L, Normando EM, Nizari S, Lara D, Cordeiro MF. Tracking longitudinal retinal changes in experimental ocular hypertension using the cSLO and spectral domain-OCT. *Invest Ophthalmol Vis Sci*. 2010;51:6504–6513.
29. Kaburaki T, Zhang Q, Jin X, et al. Effects of Japanese herbal medicine Sairei-to on murine experimental autoimmune uveitis. *Graefes Arch Clin Exp Ophthalmol*. 2013;251:2733–2739.
30. Kim M, Kim H, Kwon HJ, Kim SS, Koh HJ, Lee SC. Choroidal thickness in Behcet's uveitis: an enhanced depth imaging-optical coherence tomography and its association with angiographic changes. *Invest Ophthalmol Vis Sci*. 2013;54: 6033–6039.
31. Lardenoye CW, van Kooij B, Rothova A. Impact of macular edema on visual acuity in uveitis. *Ophthalmology*. 2006;113: 1446–1449.
32. Sen A, Paine SK, Chowdhury IH, et al. Association of interferon-gamma, interleukin-10, and tumor necrosis factor-alpha gene polymorphisms with occurrence and severity of Eales' disease. *Invest Ophthalmol Vis Sci*. 2011;52:171–178.
33. Menezo V, Lightman S. The eye in systemic vasculitis. *Clin Med (Lond)*. 2004;4:250–254.
34. Wong TY, Islam FM, Klein R, et al. Retinal vascular caliber, cardiovascular risk factors, and inflammation: the multi-ethnic study of atherosclerosis (MESA). *Invest Ophthalmol Vis Sci*. 2006;47:2341–2350.
35. Hinshaw SJ, Ogbeifun O, Wandu WS, et al. Digoxin inhibits induction of experimental autoimmune uveitis in mice, but causes severe retinal degeneration. *Invest Ophthalmol Vis Sci*. 2016;57:1441–1447.

Investigative Ophthalmology & Visual Science

Downloaded from iovs.arvojournals.org on 12/04/2020